Journal of Operation and Automation in Power Engineering

Vol. 9, No. 2, Aug. 2021, Pages: 144-159

http://joape.uma.ac.ir

A Comprehensive DC Railway Traction System Simulator Based on MATLAB: Tabriz Line 2 Metro Project Case Study

S. Razmjou

Department of Management, Faculty of Economics, Management, and Business, Tabriz Campus, University of Tabriz, Tabriz Iran.

Abstract- *As a result of rapid global urbanization, energy and environmental sustainability are becoming increasingly significant. According to the Rail Transport and Environment Report published by the International Union of Railways in 2015, energy used in the transportation sector accounts for approximately 32% of final energy consumption in the EU. Railway, representing over 8.5% of the total traffic in volume, shares less than 2% of the transport energy consumption. Railway plays an important role in reducing energy usage and CO2 emissions, compared with other transport modes such as road transport. However, despite the inherent efficiency, the energy used by the rail industry is still high, making the study of railway energy efficiency of global importance. Therefore, in this paper, the development of the comprehensive simulator software for DC-fed railway systems is demonstrated. In the proposed MATLAB based software, the train movement model and railway power network model are integrated into the simulator. This energy simulator can calculate the energy flow of the whole system according to multiple-train driving controls and timetables. Finally, the results of simulations for a standard Railway system are compared to valid references.*

Keyword: Railway systems, Traction simulation, Multi-train dynamics, Metro power system

NOMENCLATURE

A, B, C	The Davis coefficients
F	Tractive effort
F_D	Davis resistance
F_m	The maximum tractive effort
g	The acceleration due to gravity
I_{train}	Train current
I_{sub}	Traction substation current
M	The vehicle mass
M_e	The effective mass of the vehicle
M_l	The payload
M_t	The tare mass of the vehicle
P_{train}	Calculated train power
P_{el}	The train electrical power
P_{me_max}	The train maximum mechanical power
R	The vehicle resistance
s	The vehicle position along the track
t	Time
u	Binary variable
v	The train speed
V_{train}	Train voltage
Y_{bus}	Admittance matrix
Y_c	Series element admittance matrix
Y_s	Shunt element admittance matrix
α	The angle of the route slope
η	The efficiency of traction chain conversion
λ_w	The rotary allowance

Received: 25 Dec. 2020
Revised: 30 Jan. 2021
Accepted: 1 Feb. 2021
∗Corresponding author:
E-mail: razmjoo.sa@gmail.com (S. Razmjoo)
DOI: 10.22098/joape.2021.8197.1569
Applied Paper

1. INTRODUCTION

In recent decades, transportation energy and environmental sustainability have considered greatly by researchers. The intergovernmental Panel on Climate Change's Synthesis Report stated that the transport sector was responsible for about 23% of total energy-related

CO_2 emissions worldwide in 2014 [1]. In the EU, the energy consumed by transportation accounts for approximately 32% of the final end-use of energy in 2015 [2]. Although the railway has over 8.5% of total traffic in the volume of EU transport sector's, however, it includes less than 2% of the total energy consumption in this section. Compared with other transport forms, the railway plays an important role in reducing environmental impact and improving energy efficiency. By offering efficient transport with low environmental impacts, railway helps create a more sustainable approach to transport.

Metropolitan railways networks have been rising fast during recent years [3]. Urban rail transit, in general, refers to a railway system providing passenger services within metropolitan areas. Metros, light rails, tramways, and commuter rails are all different forms of urban rail transportation. The urban rail aims to transport passengers in a city quickly and easily. Hong Kong metro regularly transports 80,000 passengers per hour during peak time, which is four times higher than by bus [3]. Urban rail transit is also characterized by short headway and dwell time, and a high number of stations with short interstation distances. Urban rail systems can effectively satisfy high transportation demand and reduce air pollution in metropolitan areas. Efficient operation of a multi-train system is still a global issue, though, the railway networks are one of the most efficient forms of transport on the land. To improve sustainability, members of the International Union of Railways and Community of European Railway and Infrastructure Companies proposed a unified approach to environmental and sustainability topics in the European rail sector in 2010 [4]. They addressed four targets for the rail sector to improve performance in terms of the environment, including climate protection, energy efficiency, exhaust emissions and noise. European railway companies agreed to reduce specific average CO_2 emissions from train operation by 50% in 2030, compared to the emissions in 1990. Besides, it was agreed that by 2030 the energy consumption from train operation will be reduced by 30%, compared to the consumption in 1990. The study of innovative strategies and technologies to reduce railway energy consumption also attracts researchers across the world. Railway energy consumption optimization strategies are considered by a lot of researchers in the world. Inclusive energy-related metrics for residential rail systems have been formed to analyses the actual energy realization of the system, assess energy optimization strategies and monitor the progress of the implemented measures [5]. The current practices, strategies and technologies to reduce energy consumption are assessed by a holistic approach [6]. The energy consumption in existing urban rail systems could be reduced by approximately 25-35% by optimizing driving controls, timetables, operation strategies and energy storage devices. But the lack of comprehensive simulator software has made it a serious challenge. Most of the available software is commercial and using them needed high costs.

All electrical railway feeding networks transmit AC or DC energy through conductor systems along the track to supply electric vehicles. AC supplies are commonly used for main lines and high-speed railways, but metros, light railways, and suburban railways generally use DC supplies. Integrated AC / DC load flow analysis for simulation of traction systems has been the main goal of many studies. Ref. [7] proposed a static model for moving loads that eventually led to a set of nonlinear algebraic equations. Similarly, in Refs. [8, 9] an integrated computational method for simultaneously solving DC and AC side equations provided. In addition to the traction system, the AC \ DC load flow process is described in detail in [10-12]. To solve network equations, standard solution methods such as Newton-Raphson and Gauss-Seidel must be modified to be able to find system solutions to nonlinear traction constraints such as regenerative trains and non-receptivity. Various modelling for the traction systems has been considered in different references [13]. In most of these references, the network of the traction system is modelled by dividing the line (rail) into a limited number of segments of the same length. Each segment is considered as a π model [14, 15] or two π models [16], according to EN 50122-1 [17]. To avoid complicating the problem and increasing the accuracy of the results, a suitable solution is to perform AC load flow computations separately from the DC and exchange the results repeatedly during the simulation. This prevents divergence of AC load distribution and helps to consider the DC side model in full detail. This method was first proposed by [18].

In this paper, a MATLAB based Railway Traction System Simulator (RTSS) is proposed. The proposed RTSS integrates the single/multi-train dynamics along with DC power network simulations and provides the energy flow of the whole system according to multiple-train driving controls and timetables. The suggested RTSS calculates the voltage deviations in traction substations and according to technical metrics of the network offers the best location for traction substations. The results of the proposed method are compared with valid references for a standard test system provided by

EN-50641 British railway standard for railway simulators. The key features of the proposed RTSS are as follows:

- Using MATLAB for computations which makes it user friendly and strong capabilities.
- Integrating the dynamic analysis with DC power network simulations.
- Multi-train system simulation.
- Allocation of traction substation along the route considering technical metrics of the network.

2. Methodology

Research into the computer-based simulation of train movements and power-supply conditions has been ongoing for several decades. In 1978, a computer-based simulator was developed to study the performance characteristics of rapid-transit services [19]. This literature demonstrated the practicability of simulation techniques in solving train movement and power network issues. The linearization techniques were adopted. The application of diakoptics to solve DC railway power networks was first presented in [20]. Coupled with the sparse matrix techniques, this work improved the efficiency of solving complex railway power networks. In order to examine the non-linear power flows in electrical power networks, algebraic equations with various iterative methods were utilized and applied, for example, the Newton-Raphson iterative method, Point-Jacobi method, Zollenkopf's bifactorisation and Incomplete Cholesky Conjugate Gradient (ICCG) method [21-23].

1.1. Train Movement Modelling

1.1.1. Equations of movement

Figure 1 indicates the forces on a traction vehicle located on an uphill section of track. The tractive effort (F) applied to a vehicle is used for moving the train against the friction forces (R) and gravitational forces ($Mg\sin(\alpha)$) in moving the mass of the train uphill [24].

The train movement can be determined by standard Newtonian equations of motion. In the longitudinal direction, the motion of the vehicle is governed by the tractive effort, the gradient and the vehicle resistance [21], known as Lomonossoff's equation in (1).

$$M_e \frac{d^2 s}{dt^2} = F - Mg\sin(\alpha) - R \qquad (1)$$

Where Me is the effective mass of the vehicle [kg];s is the vehicle position along the track [m];t is the time [s]; F is the tractive effort [N]; R is the vehicle resistance [N]; M is the vehicle mass [kg]; g is the acceleration due to gravity [m/s2] andα is the angle of the route slope [rad].

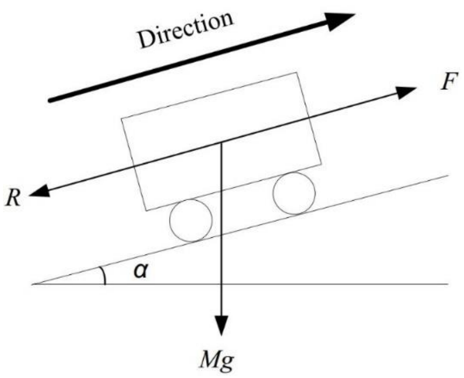

Fig. 1: Forces on a traction vehicle

The vehicle mass is the sum of the tare mass and payload in Eq. (2). When a train is accelerated linearly, the rotating parts are also accelerated in a rotational sense. The rotational effect of wheels and motors should be added into the linear train motion by increasing the effective train mass. This rotational inertia effect is called 'rotary allowance' and it is expressed as a fraction of the tare weight of the train (λw). The effective mass can be calculated by Eq. (3). The value of the rotary allowance varies from 5% to 15%, which is less for a heavy body with a small number of motored axles and more for a light body with all axles motored [25].

$$M = M_t + M_l \qquad (2)$$

$$M_e = M_t \times (1 + \lambda_w) + M_l \qquad (3)$$

Where M_t is the tare mass of the vehicle [kg]; M_l is the payload [kg] and λw is the rotary allowance. The train moves in the opposite direction to friction and aerodynamic drag. The main component of vehicle resistance is the rolling resistance, which is related to the weight, shape and speed. The formula for working out rolling resistance is known as the Davis Equation in (4). The Davis coefficients *A*, *B* and *C* are difficult to predict from theoretical calculations, which are usually determined by run-down experiments [26].

$$F_D = A + B\frac{ds}{dt} + C\left(\frac{ds}{dt}\right)^2 \qquad (4)$$

Where, F_D is Davis resistance [N]; *A* is Davis equation constant [N]; *B* is Davis equation linear term constant [N/(m/s)] and *C* is Davis equation quadratic term constant [N/(m/s)2].

1.1.2. Tractive Effort Curve

The tractive effort is produced by the traction motors and overcomes the resistance and gradient. It varies with the types of technology and motors. However, there are several common features used to generalize a tractive effort curve representing most traction systems. The tractive effort curve describes the relationship between the tractive effort and the speed of the train. Figure 2 describes the tractive effort curve of a suburban train at the nominal voltage in BS EN 50641 Railway Application – Fixed installations [27].

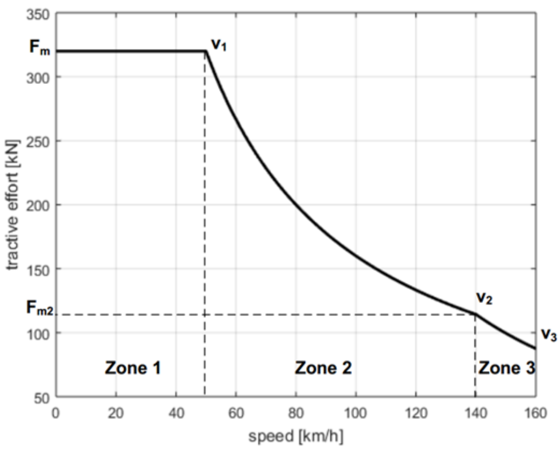

Fig. 2: Tractive effort curve of a suburban train

There are three distinct phases in the tractive effort curve. Zone 1 is characterized by constant torque operation. The tractive effort is maintained until the vehicle reaches base speed $v1$. The vehicle also reaches the maximum power at $v1$. Due to the power limitation in the onboard system, the tractive effort decreases at a rate of $1/v$ in zone 2. This is a constant power operation. At a higher speed, there is a further reduction of tractive effort at a rate of $1/v2$. This is caused by the motor limitation. The power decreases from the maximum power in zone 3, which can be called reduced power operation. Eqs. (5) and (6) are given to indicate the features of the tractive effort curve. The tractive effort can be calculated by the vehicle speed. The maximum mechanical power is given in Eq. (7).

$$F(v)=\begin{cases} F_m & v<v_1 \\ \dfrac{F_m \times v_1}{v} & v_1<v<v_2 \\ \dfrac{F_m \times v_2^2}{v^2} & v_2<v<v_3 \end{cases} \tag{5}$$

$$F_{m2}=\frac{F_m \times v_1}{v_2} \tag{6}$$

$$P_{me\_\max}=F_m \times v_1 \tag{7}$$

Where *Fm* is the maximum tractive effort [N]; *Fm2* is the tractive effort at speed *v2* [N] and *Pme_max* is the train maximum mechanical power [W].

1.1.3. Train Driving Styles

Train driving control can be generally categorized into four modes: motoring, cruising, coasting and braking [28]. The train speed trajectory can be generated by different driving strategies. Figure 3 shows an example of a speed curve with these four modes in sequence.

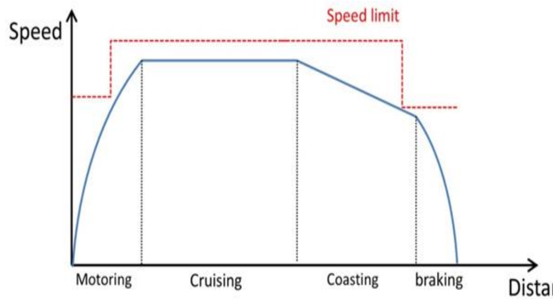

Fig. 3: Train speed curve

The motoring mode is generally active at the beginning of the journey, where it is used to increase the vehicle speed. The tractive effort in the motoring mode is normally higher than the sum of the effort by gradient and the resistance. The acceleration is positive which is given in Eq. (8).

$$\begin{cases} F>Mg\sin(\alpha)+R \\ a=\dfrac{F-Mg\sin(\alpha)-R}{Me}>0 \end{cases} \tag{8}$$

Cruising mode is invoked when the train reaches a higher speed. Partial power is adopted at this time to maintain this speed. The tractive effort in cruising mode is equal to the sum of the effort by gradient and resistance, as shown in Eq (9). The acceleration in this mode is equal to zero.

$$\begin{cases} F=Mg\sin(\alpha)+R \\ a=\dfrac{F-Mg\sin(\alpha)-R}{Me}=0 \end{cases} \tag{9}$$

When the coasting mode is applied, no traction power is required by the train. Coasting mode consumes zero traction power, which is an energy-efficient driving style. In coasting, the tractive effort is equal to zero. The acceleration is determined by the balance of the forces produced by the gradient and resistance as shown in Eq (10). The train speed normally decreases in coasting, but it may increase when the train is on a steep downhill.

$$\begin{cases} F=0 \\ a=\dfrac{0-Mg\sin(\alpha)-R}{Me}<0 \end{cases} \tag{10}$$

Braking mode is applied when the train is approaching a stop or a speed limit. In braking mode, both the tractive effort and acceleration are negative as in Eq (11).

$$\begin{cases} F < 0 \\ a = \dfrac{F - Mg\sin(\alpha) - R}{Me} < 0 \end{cases} \tag{11}$$

1.1.4. Motion Simulator Design

Figure 4 shows the diagram of the motion simulator structure. If the vehicle state at *step i* is known, and the tractive effort at *step i* is equal to *Fi*, the mechanical power required by the train in the current state is given in Eq (12).

$$P_{me\_i} = F_i \times v_i \tag{12}$$

In order to analyses the power flow in the power network simulation, the electrical power requirements can be transformed from the mechanical power results as in Eq (13). The efficiency (η) refers to the whole traction chain from the current collector to the wheel, which is around 85%. The positive mechanical power will lead to a higher positive electrical power requirement. The negative mechanical power is the braking power, which will lead to a lower electric regenerative braking power.

$$P_{el\_i} = \begin{cases} \dfrac{P_{me\_i}}{\eta} & P_{me\_i} \geq 0 \\ P_{me\_i} \times \eta & P_{me\_i} < 0 \end{cases} \tag{12}$$

Where *Pme* is the train mechanical power [W]; *Pel* is the train electrical power [W] and η is the efficiency of traction chain conversion.

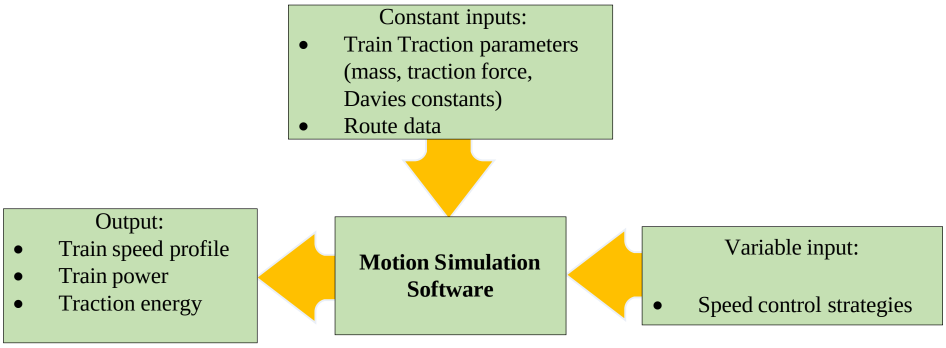

Fig. 4: Diagram of motion simulator structure

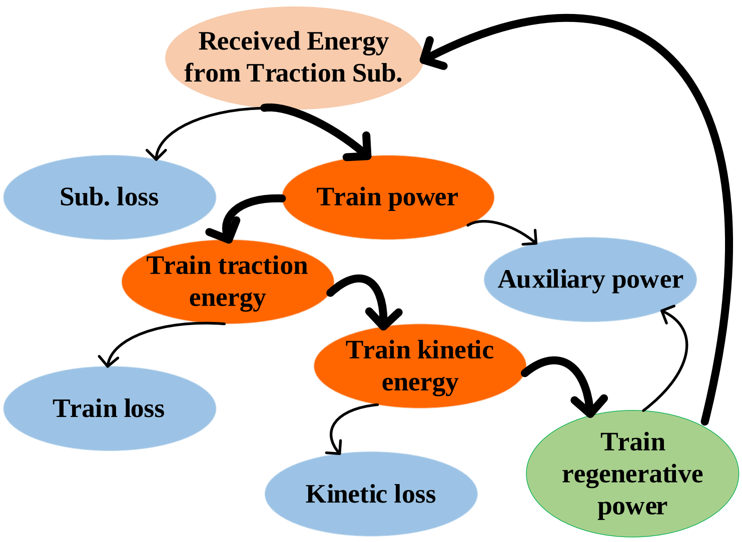

Fig. 5: The power flow diagram in the railway system

1.2. Power Network Modelling

In modern railways, the DC traction substations are normally equipped with transformers and rectifiers, drawing electricity from local distribution networks [29]. The electrical supply fed to railways is typically at 132, 66 or 33 kV AC, depending on the size and demand of railway systems.

A typical energy flow chart in railway systems is shown in Fig. 5. The electrical energy supplies come from substations. Some of the substation energy is dissipated during electricity transmission. The remaining substation energy is consumed by the train. Some of the train energy is used by the auxiliary system and the rest of train energy is used by traction. The train traction energy is dissipated during the conversion from electrical to mechanical. The train kinetic energy results in the movement. Some of the kinetic energy overcomes the motion resistance and some are regenerated during braking. The regenerated braking energy can be used by the auxiliary system directly or transferred back to the contact lines to supply other motoring trains in the network. As a result, the substation energy consumption could be reduced.

In a DC railway power network, the traction rectifier substations are the primary electricity source for vehicles. Figure 6 presents a typical DC traction power network with multiple trains on up and down tracks. The rectifier substation is connected to the DC busbar, which feeds the power network in both the up and down tracks. When the transmission line voltage is higher than the substation voltage itself, the rectifier substation will prevent current from flowing back to the AC utility grid. This section introduces the method to simulate the components in the power network by equivalent electric circuits.

1.2.1. Rectifier substations

Overall, the electrical supply substation is equipped with three-phase 6-pulse or 12-pulse rectifiers, as shown in Fig. 7. With the development of power electronic techniques, equivalent 24-pulse rectifiers are being applied in modern rapid transit systems, where two 12-pulse rectifiers are combined in parallel. The voltage regulation characteristic of the rectifier units is nonlinear, where the ratio of the output voltage to current depends on the loads [30]. In order to simplify simulation analysis, this study limits the working region of the rectifier units. Thus, the voltage regulation characteristic can be simplified as linear. For example, in Figure 7, the no-load voltage (850 V) decreases linearly with the current. The rated voltage and current are 750 V and 2500 A, respectively. The equivalent resistance for this rectifier substation can be calculated by Eq. (13).

$$R_{sub} = \frac{\Delta V}{\Delta I} = \frac{V_{noload} - V_{rated}}{I_{rated} - 0} = \frac{850-750}{2500-0} = 0.04\ \Omega \quad (13)$$

The Thevenin's and Norton's models of rectifier substation are shown in Fig. 8.

In Fig. 8, R_{big} is 10^6 and when the substation is on, u is equal to 0 or it is 1. The substation current can be calculated by Eq (14).

$$I_{sub} = \frac{V_{sub}}{R_{sub} + u \times R_{big}} \quad (14)$$

1.2.2. Dynamic Train Loads

Some previous research used constant current source models or constant efficiency of regenerative braking energy usage to present trains in a traction power network [31-34]. However, this is not accurate in the study of energy consumption for railways. In railway power systems, modern trains collect electricity behaving as voltage-dependent power loads. The power consumed by trains does not depend on the voltage or current at the pantograph [13]. In this paper, trains are considered as dynamical power sources or power loads for better simulation performance. The power network simulator will solve the power flow. The train voltage and current can be calculated. $Ptrain$ is the electric power which the traction train receives or the braking train exports, given in Eq. (15). If the train is running in a normal mode, the final train electric power is equal to the train power demand.

$$P_{train} = I_{train} \times V_{train} \quad (15)$$

The equivalent circuit of the train in motoring and braking modes are shown in Fig. 8.

1.2.3. Admittance Matrix Construction

An example of the railway system equivalent circuit is described in Fig. 9, which consists of the equivalent models of substations and trains. The paralleling post connects the contact lines on both tracks for reducing transmission losses as well as improving line voltages. It is modelled by a zero-resistance conductor connecting two contact lines. The substation connects with the busbar to feed both tracks. In practice, the rails bond together every 250 or 500 meters. Two tracks can be modelled by one combined return rail for admittance simplification with a reasonably low error [35]. The conductor resistors are used to represent the overhead line and return running rail resistance, which is split by trains, substations and parallel posts. The resistance of the contact line and lumped rail depends on the length and resistivity of the conductor as in Eq. (16), where ρ_c and ρ_r refer to the resistivity of the contact line and return rail per track. The resistivity of overhead conductor systems is in the range of 30 to 90 mΩ/km, whereas it is between 8 and 20 mΩ/km for the third rail [36, 37]. The resistivity of the return rail is around 20 mΩ/km/track [27].

$$\begin{cases} R_c = L \times \rho_c \\ R_r = L \times \dfrac{\rho_r}{2} \end{cases} \quad (16)$$

The admittance matrix of a railway power network circuit is complex. With the chain circuit topology of railway equivalent circuit, the admittance matrix can be constructed conveniently [38]. Figure 10 describes a chain circuit topology of railway equivalent circuit with 3 paralleling layers. The circuit is classified by N-1 serial conductors and N shunt sections. The serial conductors represent the split resistances of contact lines and lumped rails. The shunt sections include the parallel posts, substations and trains, which can separate the conductor lines. The nodal analysis equation can be applied to solve the power flow of the railway network in Eq. (17). The admittance matrix of the whole network (Y) is a 3N×3N matrix, while both the current and voltage vector is a 1×3N matrix.

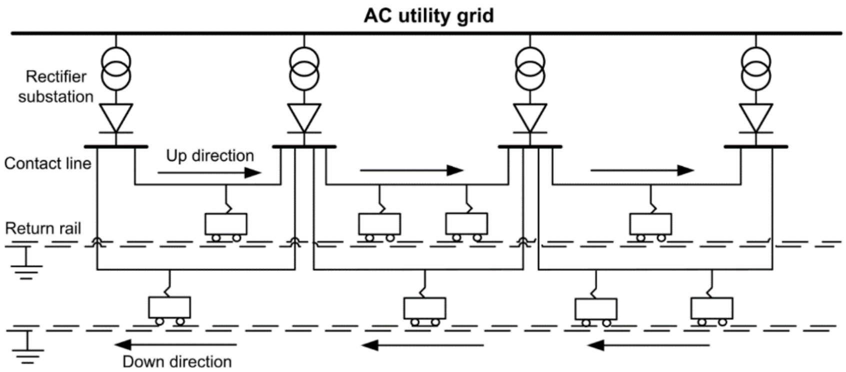

Fig. 6: A typical DC traction power network

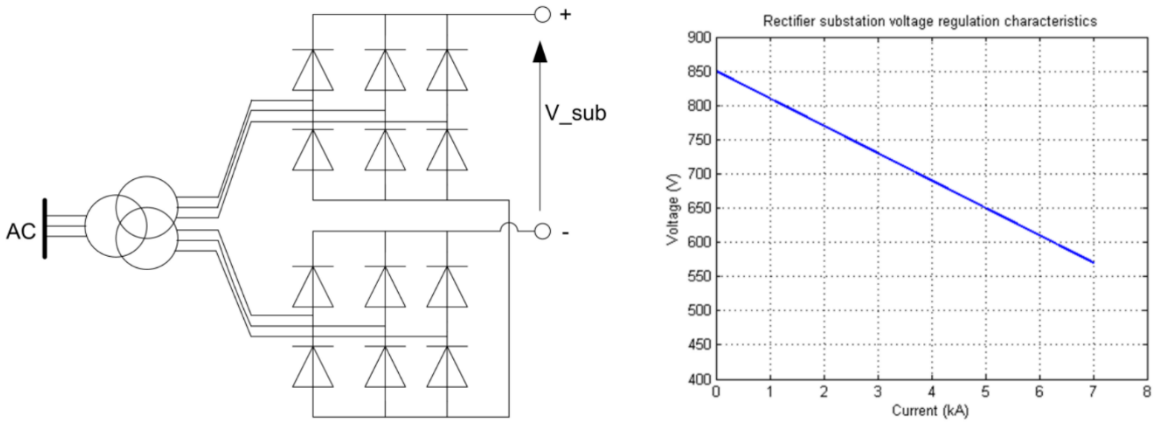

Fig. 7: 12-pulse rectifier with corresponding voltage characteristic

$$I = Y \times V \quad (17)$$

$$Y = \begin{bmatrix} Y_{s1}+Y_{c1} & -Y_{c1} & 0 & & & \\ -Y_{c1} & Y_{c1}+Y_{s2}+Y_{c2} & -Y_{c2} & \cdots & 0 & \\ 0 & -Y_{c2} & Y_{c2}+Y_{s3}+Y_{c3} & & & \\ & \vdots & & \ddots & \vdots & \\ & 0 & & \cdots & Y_{cN-2}+Y_{sN-1}+Y_{cN-1} & -Y_{cN-1} \\ & & & & -Y_{cN-1} & -Y_{cN-1}+Y_{sN} \end{bmatrix} \quad (18)$$

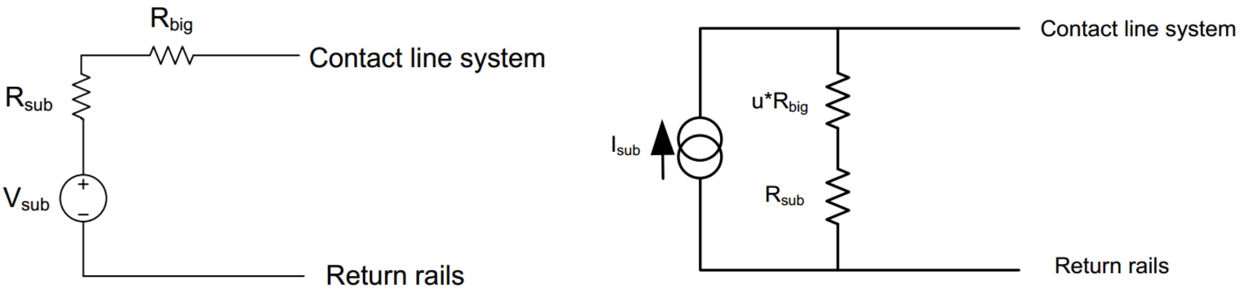

a b

Fig. 8: Equivalent model of a rectifier, a) Thevenin's model; b) Norton's model

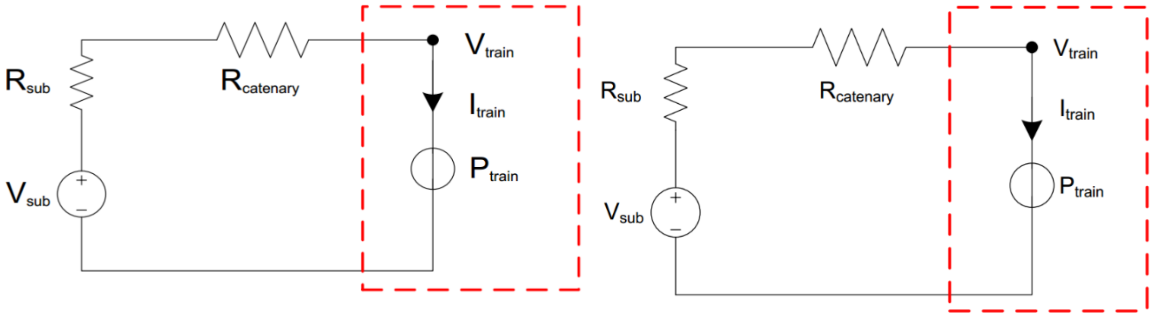

a) Motoring train **b) Braking Train**

Fig. 9: Equivalent model Train

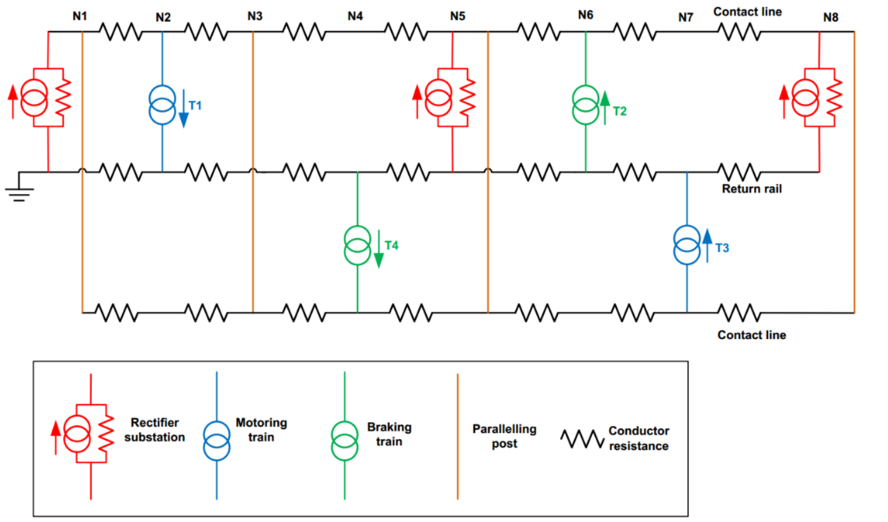

Fig. 10: Railway system equivalent circuit

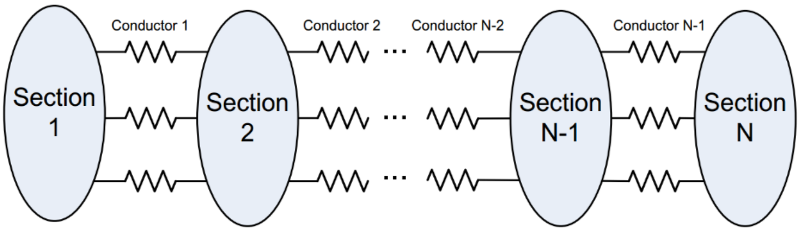

Fig. 11: Chain circuit topology of railway equivalent circuit

Matrix Y is composed of the admittance matrix of each serial conductor element (Yc) and shunt element (Ys), which are 3×3 matrices. The admittance matrix of the whole network is expressed in Eq. (18), which is a sparse matrix. The current and voltage vectors in Eq. (17) are both 1×3N matrices, which are composed of nodal voltage vector (Vs) and current vectors (Is) of each shunt section, as in Eq. (19) and (20). Both Vs and Is are 1×3 matrices. According to the features of the railway power network, the serial and shunt elements can be concluded by the following forms.

$$V = \begin{bmatrix} V_{s1} \\ V_{s2} \\ V_{s3} \\ \vdots \\ V_{sN-1} \\ V_{sN} \end{bmatrix} \tag{19}$$

$$I = \begin{bmatrix} I_{s1} \\ I_{s2} \\ I_{s3} \\ \vdots \\ I_{sN-1} \\ I_{sN} \end{bmatrix} \tag{20}$$

The serial conductors consist of the contact lines and the lumped rails. The resistance can be calculated by Eq. (16). The admittance matrix of on series part can be expressed in Eq. (21).

$$Y_c = \begin{bmatrix} \frac{1}{R_1} & 0 & 0 \\ 0 & \frac{1}{R_2} & 0 \\ 0 & 0 & \frac{1}{R_3} \end{bmatrix} \tag{21}$$

The shunt resistance is a basic model for the shunt section, which connects paralleling conductor lines. The admittance for this element is expressed in Eq. (22). The self-admittances (Ys11 and Ys22) and the mutual admittances (Ys12 and Ys21) are equal to 1/R.

$$Y_s = \begin{bmatrix} \frac{1}{R} & -\frac{1}{R} & 0 \\ -\frac{1}{R} & \frac{1}{R} & 0 \\ 0 & 0 & 0 \end{bmatrix} \tag{22}$$

The parallel post which connects two contact lines. According to the admittance matrix structure of shunt resistance, the parallel post can be assumed as a very small resistor connecting both contact lines. Therefore, the admittance matrix of the parallel post can be expressed in Eq. (23), where the small resistance (R_{small}) is set to 10^{-6} Ω in this paper [39].

$$Y_s = \begin{bmatrix} \frac{1}{R_{small}} & 0 & -\frac{1}{R_{small}} \\ 0 & 0 & 0 \\ -\frac{1}{R_{small}} & 0 & \frac{1}{R_{small}} \end{bmatrix} \tag{23}$$

Similarly, for a grounding connection, the admittance matrix can be written as in Eq. (24). The self-admittance Ys22 is equal to 1/R_{small}, while all the mutual admittances are equal to zero.

$$Y_s = \begin{bmatrix} 0 & 0 & 0 \\ 0 & \frac{1}{R_{small}} & 0 \\ 0 & 0 & 0 \end{bmatrix} \tag{24}$$

The substation is composed of a current source, a resistance and parallel post. The ideal current source does not affect the admittance matrix. The admittance matrix of a substation can be calculated by Eq. (25), which is the sum of the admittance matrix of shunt resistance and parallel post. The current vector of the substation can be calculated according to the substation current, as in Eq. (26). *Is_sub11*, *Is_sub12* and *Is_sub13* are the currents flowing through line 1, line 2 and line 3, respectively.

$$Y_{sub} = \begin{bmatrix} \frac{1}{R_{sub}} & -\frac{1}{R_{sub}} & 0 \\ -\frac{1}{R_{sub}} & \frac{1}{R_{sub}} & 0 \\ 0 & 0 & 0 \end{bmatrix} + \begin{bmatrix} \frac{1}{R_{small}} & 0 & -\frac{1}{R_{small}} \\ 0 & 0 & 0 \\ -\frac{1}{R_{small}} & 0 & \frac{1}{R_{small}} \end{bmatrix} \tag{25}$$

$$I_{s\_sub} = \begin{bmatrix} I_{sub} \\ -I_{sub} \\ 0 \end{bmatrix} \tag{26}$$

Since the model of the trains in normal operation does not consist of resistance, the admittance matrix is null in Eq. (27). For the traction train in up-direction, the train collects the current from the up-tract contact line and the current returns back to lumped rails. Therefore, the current vector can be expressed in Eq. (28). As for the braking train, the braking train regenerates power and feeds the contact lines. Therefore, the current vector can be expressed in Eq. (29).

$$Y_{train} = \begin{bmatrix} 0 & 0 & 0 \\ 0 & 0 & 0 \\ 0 & 0 & 0 \end{bmatrix} \tag{27}$$

$$I_{t\_trac\_up} = \begin{bmatrix} -I_{train} \\ I_{train} \\ 0 \end{bmatrix} \tag{28}$$

$$I_{t\_brake\_up} = \begin{bmatrix} I_{train} \\ -I_{train} \\ 0 \end{bmatrix} \tag{29}$$

Table 1: Test case 1 station location

Station no#	Station label	Station location (m)
1	S1	0
2	S2	1334
3	S3	2620
4	S4	4706
5	S5	6971
6	S6	9309
7	S7	10663
8	S8	11943
9	S9	13481
10	S10	14474
11	S11	16456
12	S12	18822
13	S13	20097
14	S14	22728

1.2.4. Load Flow Solver

The railway system equivalent circuit is made up of the voltage sources and resistance, which are linear components, a power source (train) which is a nonlinear component, as well as the diode which is a piecewise component. To solve the load flow problem for the railway power network, an iterative method with piecewise analysis is required. In this research, the current-vector iterative method is used to obtain an accurate solution for a DC-fed railway network. The load power flow analysis aims to find the solution with higher train voltage, which is the actual train voltage in the railway network. The pseudo-code of the current-vector iterative method is presented in Fig. 11.

***Step* 1:** *Initialize all the train voltage by the no-load voltage of the substation as in Eq.* (30).

$$V_{train\_n}^{(0)} = V_{sub} \tag{30}$$

***Step* 2:** *Calculate the train currently at the next iteration by Eq.* (31).

$$I_{train\_n}^{(1)} = \frac{P_{train\_demand\_n}}{V_{train\_n}^{(0)}} \tag{31}$$

***Step* 3:** *Update nodal voltages by nodal analysis by Eq.* (32). *The train voltage at this iteration can be updated at this step. The nodal analysis Eq.* (32) *is equivalent to Eq. (33) which is obtained from the Thevenin's equivalent circuit.*

$$[V]^{(1)} = [Y]^{-1} \times [I]^{(1)} \tag{32}$$

$$V_{train\_n}^{(1)} = V_{eq\_n} - r_{eq} \times I_{train\_n}^{(1)} \tag{33}$$

***Step* 3:** *Calculate train power at this iteration by Eq.* (34).

$$P_{train\_n}^{(1)} = V_{train\_n}^{(1)} \times I_{train\_n}^{(1)} \tag{34}$$

***Step* 3:** *Check whether the difference of calculated train power and train power demand is within the criteria. If so, the current-vector iterative method ends. If not, repeat **Step** 2 using the updated train voltage.*

Fig. 11: The pseudo-code of the current-vector iterative method

3. Simulation Results

3.1. Dynamic simulation validation

3.1.1. *Test case 1*

The Beijing Yizhuang Subway Line (BYSL) in China has been in operation since 2010. It is a significant subway line which links the suburbs of Beijing and the city Centre with a length of 22.73 km. This system has 14 stations whose locations are shown in Table 1. Figure 12 shows the location of stations along the route. The maximum speed of the train on this route is 80 km/s.

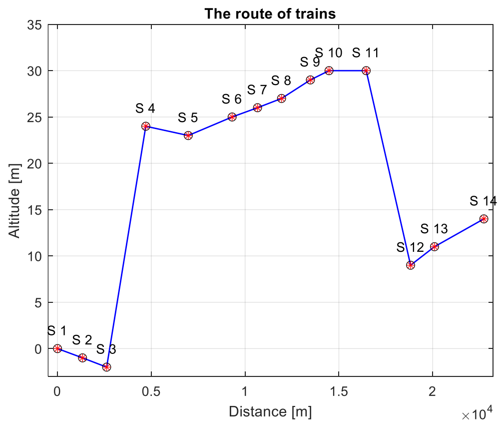

Fig. 12: Route vertical alignment and train station location

The train operated in the Beijing Yizhuang Subway

Line is formatted by 6 carriages with 3M3T topology. 3 of them are equipped with motors (M1 to M3), while the other carriages are trailers (T1 to T3). The tare weight of each carriage is shown in Table 2.

Table 2: Vehicle tare mass [tones]

Car No.	T1					
Vehicle tare mass	33	35	28	35	33	35	199

The passenger weight of each carriage for different scenarios is presented in Table 3.

Table 3: Passenger mass [tones]

Car No.	T1	M1	T2	M2	T3	M3	Tot
AW0 (no load)	0	0	0	0	0	0	0
AW2 (normal load)	13.56	15.24	15.24	15.24	13.56	15.24	88.08
AW3 (over load)	17.40	19.5	19.5	19.5	17.40	19.5	112.80

The tractive parameters for different scenarios of BYSL are shown in Table 4. The tractive effort curve in Fig. 13 describes the relationship between tractive effort and velocity in different scenarios.

Table 4: Tractive characteristics

-	F_m[kN]	F_{m2}[kN]	V_1 [km/h]	V_2 [km/h]
AW0 (no load)	200	200	51.3	51.3
AW2 (normal load)	289	228.8	38	48
AW3 (over load)	312	228.8	35.2	48

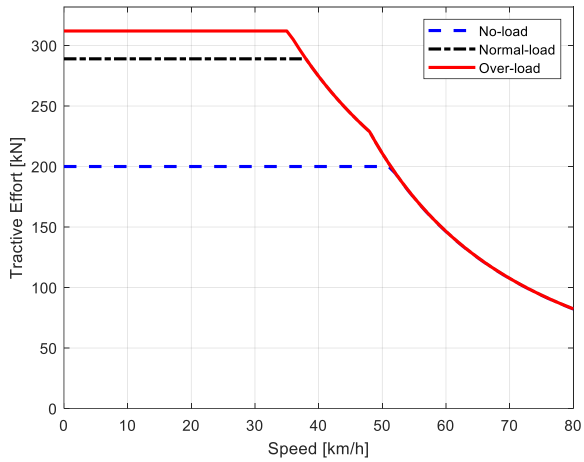

Fig. 13: Tractive effort curve

The regenerative braking effort characteristic is given in Table 5 and the braking effort curve is described in Fig. 14.

Table 5: Regenerative braking effort characteristics

-	F_m[kN]	F_{m2}[kN]	V_1 [km/h]	V_2 [km/h]
AW0 (no load)	167	167	77.8	77.8
AW2 (normal load)	239	232	64	66
AW3 (over load)	255	232	60	66

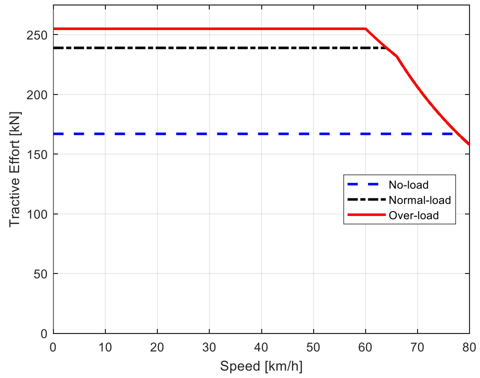

Fig. 14: Regenerative braking effort curve

The Davis coefficients for different scenarios are shown in Table 6.

Table 6: Davis constants

-	A [kN]	B [kN/(km/h)]	C [kN/(km/h)2]
AW0 (no load)	2.4180	0.0280	0.0006575
AW2 (normal load)	3.4818	0.0403	0.0006575
AW3 (over load)	3.7799	0.0437	0.0006575

The dynamic simulations of the proposed test case are extracted for single-train, in scenario AW2 without regeneration and shown in Figs. 15-18.

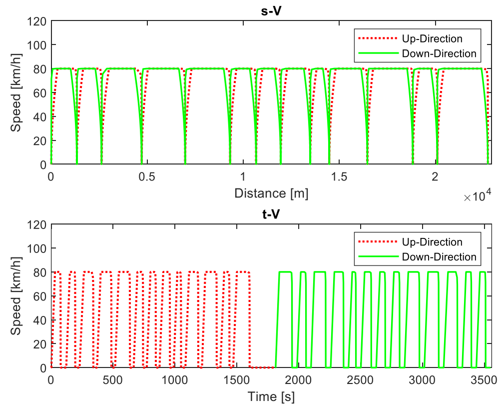

Fig. 15: Train speed vs. location and time in both up and down directions

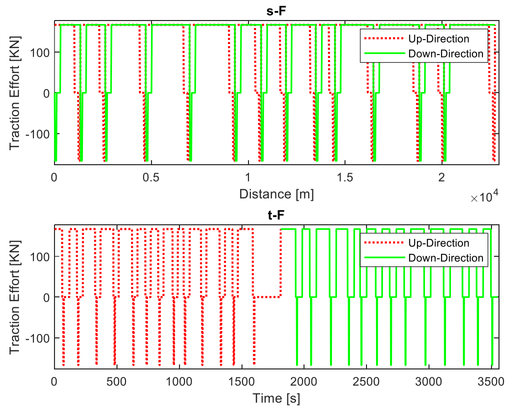

Fig. 16: Train tractive effort vs. location and time in both up and down directions

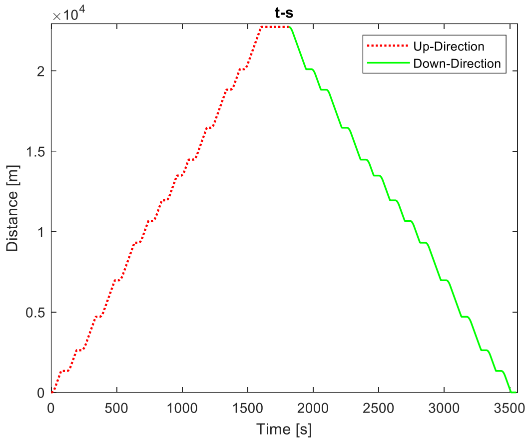

Fig. 17: Train location vs. time in both up and down directions

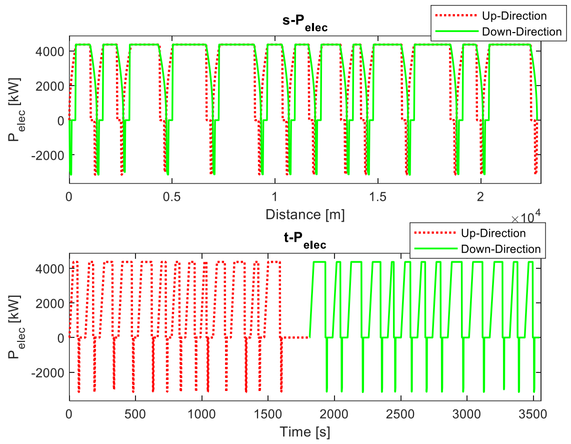

Fig. 18: Train Pelec vs. location and time in both up and down directions

In the following, it is assumed that the test system of the previous section has 44 (similar) trains with the headway of 90 seconds. The movement graphs of trains in this system are presented in Fig. 19, where regeneration is not considered and the condition of passengers is in a normal state (AW2).

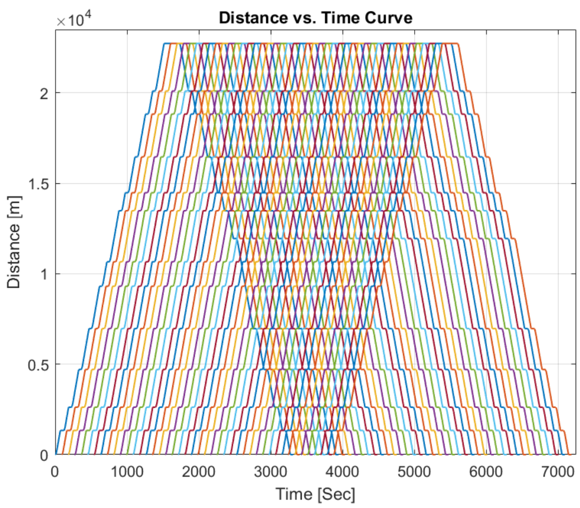

Fig. 19: Trains location vs. time

3.2. Power flow solver validation

The fixed data of the train and power network for the test is shown in Table 7. The power network data is collected from BS-EN50641 British Standard in Railway Applications- Fixed installations [27]. The dynamic data including train location and power demand can lead to different results. The results are validated compare to [40] and TINA, which is a circuit simulator.

The train location and power demand are assumed as dynamic inputs in this validation test. Regarding the normal traction and regeneration test, the train data is presented in Table 8. There are four trains in the power network. Two trains are motoring, and the other two are braking.

Table 7: Fixed data for the load flow solver validation test

Item	Value	Unit
Route length	8000	m
Substation No. 1 position	0	m
Substation No. 2 position	5000	m
Substation No. 3 position	8000	m
Paralleling post position	2500	m
Traction system nominal voltage	1500	V
Substation no-load voltage	1800	V
Substation source resistance	0.01	Ω
Highest permanent voltage Vmax1	1850	V
Highest non-permanent voltage Vmax2	1950	V
Under-voltage limitation	1350	V
Contact line system resistance	29	mΩ/ km/track
Return rail system resistance	20	mΩ/ km/track
Train maximum electric power	8000	KW

Table 8: Train data inputs for the load flow solver validation test

	Location [m]	Power [kW]
Train_up1	1000	8000
Train_up2	7000	8000
Train_down1	3000	-3000
Train_down2	6000	-3000

The results from the proposed RTSS simulator are presented in Table 9. The voltage, current and power of trains and substations are obtained. All the trains and substations are working in normal mode. In order to validate the simulation results, the solutions of [27] and TINA are also presented in Table 9. The current and power results from TINA and [27] are almost the same with the results from the proposed RTSS simulator. The average power difference is within 0.0043%. This proves the accuracy of the proposed RTSS power network simulator.

3.2. Tabriz metro line 2 (TML2) project

In this section, the data of the TML2 project are analyzed using the proposed RTSS simulator and the dynamic and electrical graphs are plotted. TML2 project is consist of 33 trains in a route with 28.986 km length. The headway of the system is 120 seconds and the station location are shown in Fig. 20. The train tractive effort in TML2 is presented in Fig. 21. The movement timetable of trains in TML2 project is presented in Fig. 22 for a sample time during the simulation process.

Table 9: Results for the load flow solver validation test

	Results from the proposed RTSS simulator			Results from [27]			Results from TINA		
Number of iterations	**6**			7			-		
Power mismatch	**0.0043%**			0.07%			-		
	Voltage [V]	**Current [A]**	**Power [kW]**	**Voltage [V]**	**Current [A]**	**Power [kW]**	**Voltage [V]**	**Current [A]**	**Power [kW]**
Train_up1	**1579.7**	**5064**	**7999.7**	1654	4838	8002	1654	4840	8005
Train_up2	**1660.3**	**4818.5**	**8000**	1661	4816	7999	1661	4820	8006
Train_down1	**1892**	**-1585.7**	**-3000**	1794	-1672	-3000	1794	-1670	-2996
Train_down2	**1847.1**	**-1624.2**	**-3000**	1813	-1655	-3001	1813	-1660	-3010
Substation No. 1	**1792.2**	**2680**	**4803.1**	1770	3025	5354	1770	3020	5345
Substation No. 2	**1778.8**	**718.7**	**1390.4**	1791	859	1538	1790	859	1538
Substation No. 3	**1792.2**	**2121.7**	**3802.4**	1776	2449	4349	1770	2440	4319

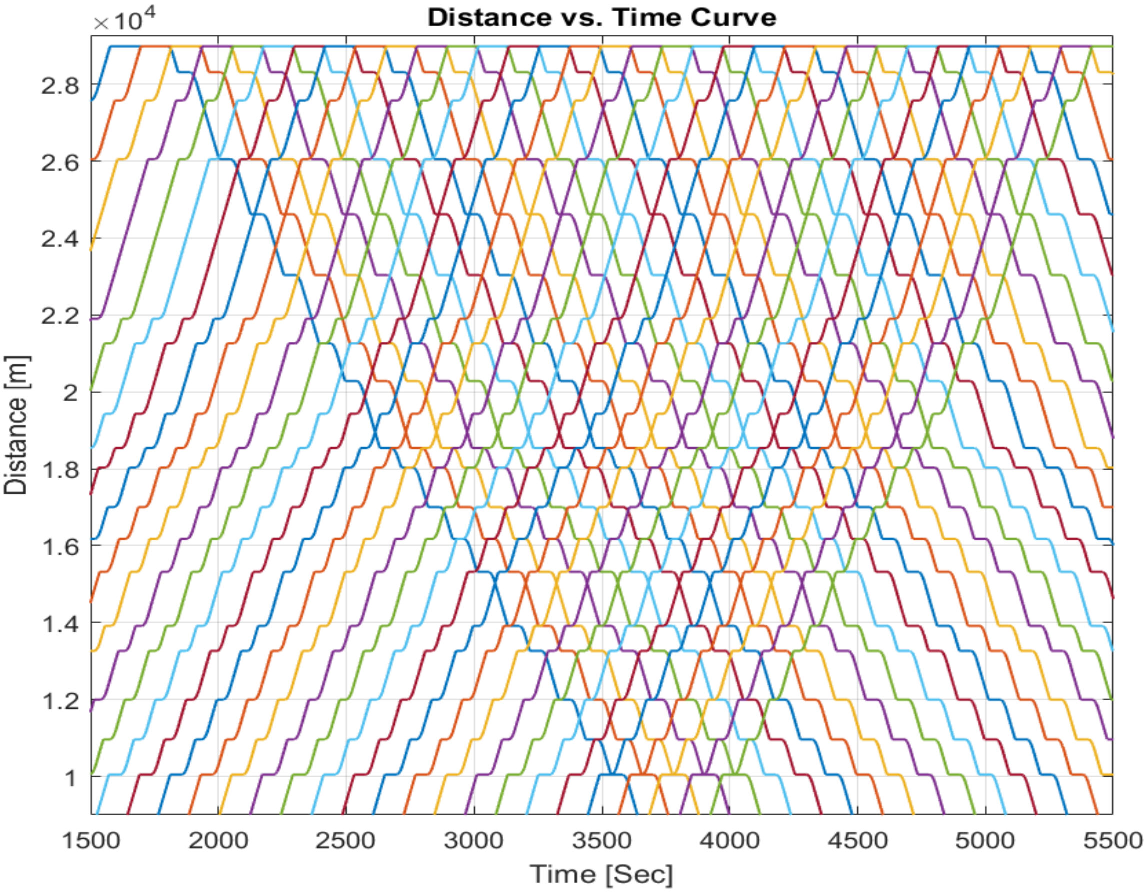

Fig. 22: The movement timetable of trains in TML2

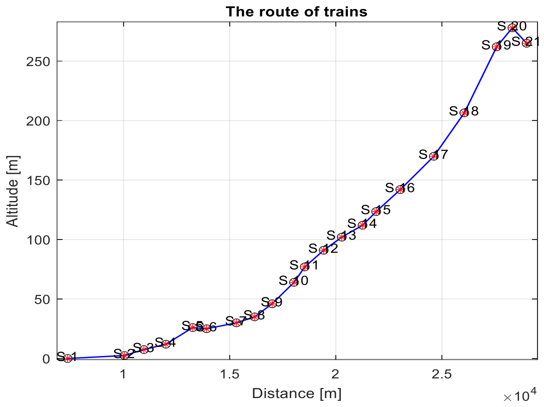

Fig. 20: Location of passenger stations in TML2 project

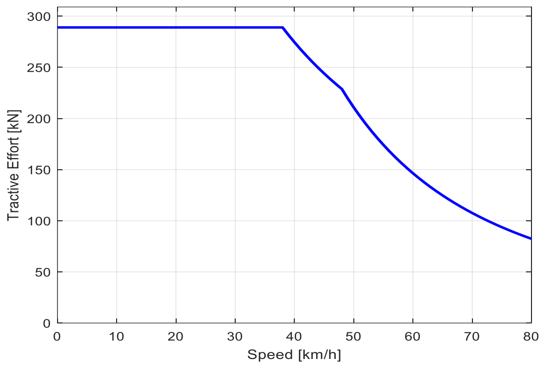

Fig. 21: Train tractive effort of TML2

Finally, the train voltage and currents are presented in Figs. 23-24. The results are obtained step by step by the proposed RTSS simulator.

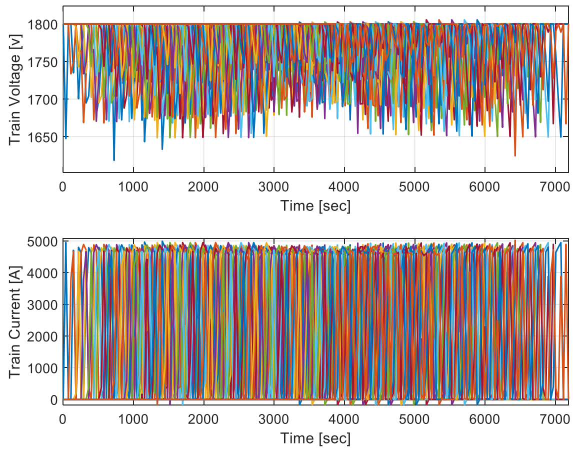

Fig. 23: Train voltages and currents in TML2

4. Conclusions

The main objective of this paper was to develop a MATLAB-based software that receives traction system fixed and variable data and performs the dynamic and DC power network analysis.

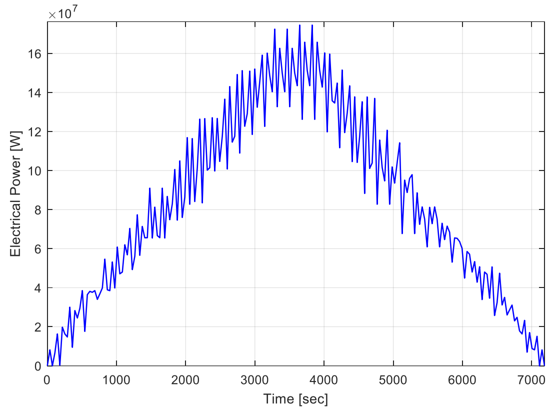

Fig. 23: Train power demand in TML2

The proposed Railway traction system simulator (RTSS), consists of three main parts, which are: dynamic analysis of the single-train system, dynamic analysis of the multi-train system, and solving the DC power network problem dynamically in the multi-train system. It should be noted that in each part of the simulation, the results obtained in the previous step are received and analyzes are performed based on them. This software first simulates the dynamics of single-train and multi-train systems based on dynamic equations and the mechanical power of trains and their position by considering three scenarios of unloaded (low passenger hours), medium load (normal passenger hours) and heavy load (passenger peak hours) during the scheduling program. Then in the next step, the mechanical power of the trains is converted to electrical power based on their efficiency and DC analysis is performed based on the electric power of the trains, the power of the auxiliary system. The information used in this project is collected from numerous articles and technical reports, all of which are listed in the list of sources. The obtained software is very simple and efficient and simulates under the powerful MATLAB software. The capabilities of this software are very high processing speed, the possibility of changing all system parameters and the possibility of optimization.

References

[1] O. Edenhofer, *Climate change 2014: mitigation of climate change* vol. 3: Cambridge University Press, 2015.

[2] R. Transport, "Environment: Facts & Figures," *Commun. Europ. Rail. Infras. Co.*, 2015.

[3] P. Fouracre, C. Dunkerley, and G. Gardner, "Mass rapid transit systems for cities in the developing world," *Trans. Rev.*, vol. 23, pp. 299-310, 2003.

[4] J. Kettner, "Moving towards sustainable mobility a strategy for 2030 and beyond for the European railway sector." *12 UIC Sust. Conf.*,Venice, 2012.

[5] A. González-Gil, R. Palacin, and P. Batty, "Optimal energy management of urban rail systems: Key performance indicators," *Energy Conv.. Manag.*, vol. 90, pp. 282-291, 2015.

[6] A. González-Gil, R. Palacin, P. Batty, and J. P. Powell, "A systems approach to reduce urban rail energy consumption," *Energy Conv. Manag.*, vol. 80, pp. 509-524, 2014.

[7] S. N. Talukdar and R. L. Koo, "The analysis of electrified ground transportation networks," *IEEE Trans. Power Appar. Syst.*, vol. 96, pp. 240-247, 1977.

[8] Y. S. Tzeng, R. N. Wu, and N. Chen, "Unified AC/DC power flow for system simulation in DC electrified transit railways," *IEE Proc. – Electr. Power Appl.*, vol. 142, pp. 345-354, 1995.

[9] T. Yii-Shen, C. Nanming, and W. Ruay-Nan, "A detailed R-L fed bridge converter model for power flow studies in industrial AC/DC power systems," *IEEE Trans. Ind. Electron.*, vol. 42, pp. 531-538, 1995.

[10] D. A. Braunagel, L. A. Kraft, and J. L. Whysong, "Inclusion of DC converter and transmission equations directly in a Newton power flow," *IEEE Trans. Power Appar. Syst.*, vol. 95, pp. 76-88, 1976.

[11] D. J. Tylavsky, "A Simple Approach to the Solution of the ac-dc Power Flow Problem," *IEEE Trans. Edu.*, vol. 27, pp. 31-40, 1984.

[12] D. J. Tylavsky and F. C. Trutt, "The Newton-Raphson Load Flow Applied to AC/DC Systems with Commutation Impedance," *IEEE Trans. Ind. Appl.*, vol. IA-19, pp. 940-948, 1983.

[13] C. J. Goodman, L. K. Siu, and T. K. Ho, "A review of simulation models for railway systems," *Int. Conf. Develop. Mass Transit Syst. Publ. No. 453)*, 1998, pp. 80-85.

[14] Y. Cai, M. R. Irving, and S. H. Case, "Modelling and numerical solution of multibranched DC rail traction power systems," *IEE Proc. – Electr. Power Appl.*, vol. 142, pp. 323-328, 1995.

[15] Y. Cai, M. R. Irving, and S. H. Case, "Iterative techniques for the solution of complex DC-rail-traction systems including regenerative braking," *IEE Proc. Gener., Transm. Distrib.*, vol. 142, pp. 445-452, 1995.

[16] C. L. Pires, S. I. Nabeta, and J. R. Cardoso, "ICCG method applied to solve DC traction load flow including earthing models," *IET Electr. Power Appl.*, vol. 1, pp. 193-198, 2007.

[17] "Railway applications – fixed installations Part 1," *Protec. Prov. Relat. Electr. Safety Earth.*, ed. Brussels: CENELEC, 1998.

[18] Shao Z.Y., Chan W.S., Allan J., and M. B., "A new method of DC power supply modelling for rapid transit railway system simulation," *Int. Conf. Computer Aided Design, Manufac. Oper. Rail. Other Mass Transit Syst.*, 1994.

[19] B. Mellitt, C. J. Goodman, and R. I. M. Arthurton, "Simulator for studying operational and power-supply conditions in rapid-transit railways," *Proc. Instit. Electr. Eng.*, vol. 125, pp. 298-303, 1978.

[20] C. J. Goodman and L. K. Sin, "DC railway power network solutions by diakoptics," *Proc. IEEE/ASME Joint Railroad Conf.*, 1994, pp. 103-110.

[21] S. Hillmansen, "Electric railway traction systems and techniques for energy saving," *IET Prof. Develop. Course Electr. Traction Syst.*, 2012, pp. 19-23.

[22] S. Hillmansen and C. Roberts, "Energy storage devices in hybrid railway vehicles: A kinematic analysis," *Proc. Instit. Mechanic. Eng., Part F: J. Rail Rapid Transit*, vol. 221, pp. 135-143, 2007.

[23] R. Takagi and T. Amano, "Optimisation of reference state-of-charge curves for the feed-forward charge/-discharge control of energy storage systems on-board DC electric railway vehicles," *IET Electr. Syst. Transport.*, vol. 5, pp. 33-42, 2015.

[24] R. J. Hill, "Electric railway traction. I. Electric traction and DC traction motor drives," *Power Eng. J.*, vol. 8, pp. 47-56, 1994.

[25] C. J. Goodman, "Overview of electric railway systems and the calculation of train performance," 9th *Instit. Eng. Tech. Prof. Develop. Course Electr. Traction Syst.*, 2006, pp. 1-24.

[26] B. P. Rochard and F. Schmid, "A review of methods to measure and calculate train resistances," *Proc. Instit. of Mechanic. Eng., Part F: J. Rail Rapid Transit*, vol. 214, pp. 185-199, 2000.

[27] B. BS-EN50641, "Railway applications-Fixed installations - Requirements for the validation of simulation tools used for the design of traction power supply systems," ed: BSI, 2014.

[28] Z. Tian, S. Hillmansen, C. Roberts, P. Weston, N. Zhao, L. Chen, *et al.*, "Energy evaluation of the power network of a DC railway system with regenerating trains," *IET Electr. Syst. Transport.*, vol. 6, pp. 41-49, 2016.

[29] R. D. White, "DC ELECTRIFICATION SUPPLY SYSTEM DESIGN," 3*rd IET Prof. Develop. Course Rail. Electr. Infrast. Syst.*, 2007, pp. 35-62.

[30] P. Pozzobon, "Transient and steady-state short-circuit currents in rectifiers for DC traction supply," *IEEE Trans. Vehic. Technol.*, vol. 47, pp. 1390-1404, 1998.

[31] T. Ratniyomchai, S. Hillmansen, and P. Tricoli, "Energy loss minimisation by optimal design of stationary supercapacitors for light railways," *Int. Conf. Clean Electr. Power*, 2015, pp. 511-517.

[32] T. Ratniyomchai, S. Hillmansen, and P. Tricoli, "Optimal capacity and positioning of stationary supercapacitors for light rail vehicle systems," *Int. Sym.*

Power Electron., Electr. Drives, Auto. Motion, 2014, pp. 807-812.

[33] X. Li and H. K. Lo, "An energy-efficient scheduling and speed control approach for metro rail operations," *Transport. Res. Part B: Methodological*, vol. 64, pp. 73-89, 2014.

[34] X. Li and H. K. Lo, "Energy minimization in dynamic train scheduling and control for metro rail operations," *Transport. Res. Part B: Methodological*, vol. 70, pp. 269-284, 2014.

[35] A. Finlayson, C. Goodman, and R. White, "Investigation into the computational techniques of power system modelling for a DC railway," 2006.

[36] F. Schmid and C. J. Goodman, "Electric railway systems in common use," 5th *IET Prof. Develop. Course Rail. Electr. Infrast. Syst.*, 2011, pp. 1-15.

[37] M. Chymera and C. J. Goodman, "Overview of electric railway systems and the calculation of train performance," *IET Prof. Develop. Course Electr. Traction Syst.*, 2012, pp. 1-18.

[38] W. Mingli, C. Roberts, and S. Hillmansen, "Modelling of AC feeding systems of electric railways based on a uniform multi-conductor chain circuit topology," 2010.

[39] C. Goodman, "Modelling and simulation," 2007.

[40] Z. Tian, "System energy optimisation strategies for DC railway traction power networks," University of Birmingham, 2017.